Molecular Therapy
Nucleic Acids
Original Article

Circular RNA circPSD3 alleviates hepatic fibrogenesis by regulating the miR-92b-3p/Smad7 axis

Fang-tian Bu,[1,2,3,5] Yan Zhu,[1,4,5] Xin Chen,[1,2,3,5] Ao Wang,[1,2,3] Ya-fei Zhang,[1,2,3] Hong-mei You,[1,2,3] Yang Yang,[1,2,3] Ya-ru Yang,[1,2] Cheng Huang,[1,2,3] and Jun Li[1,2,3]

[1]Inflammation and Immune Mediated Diseases Laboratory of Anhui Province, Anhui Institute of Innovative Drugs, School of Pharmacy, Anhui Medical University, Hefei, Anhui Province 230032, China; [2]The Key Laboratory of Anti-inflammatory and Immune Medicines, Ministry of Education, Hefei, Anhui Province 230032, China; [3]Institute for Liver Diseases of Anhui Medical University, Hefei, China; [4]The First Affiliated Hospital of Anhui Medical University, Hefei, Anhui Province 230032, China

Recently, circular RNAs (circRNAs) have been frequently reported to be involved in hepatocellular carcinoma (HCC) development and progression. However, the role of circRNAs in hepatic fibrosis (HF) is still unclear. Our previous high-throughput screen revealed changes in many circRNAs in mice with carbon tetrachloride (CCl_4)-induced HF. For instance, the expression of circPSD3, a circRNA derived from the Pleckstrin and Sec7 domain-containing 3 (PSD3) gene, was considerably downregulated in primary hepatic stellate cells (HSCs) and liver tissues of mice with CCl_4-induced HF compared to those in the vehicle group. *In vivo* overexpression of circPSD3 using AAV8-circPSD3 arrested the deterioration of CCl_4-induced HF as indicated by reduced serum alanine aminotransferase (ALT) and aspartate aminotransferase (AST) content, liver hydroxyproline level, collagen deposition, and pro-fibrogenic gene and pro-inflammatory cytokine levels. Moreover, *in vitro* loss-of-function and gain-of-function analyses suggested that circPSD3 inhibited the activation and proliferation of HSCs. Mechanistically, circPSD3 served as a sponge for miR-92b-3p, subsequently promoting the expression of Smad7. In conclusion, our present findings reveal a novel mechanism by which circPSD3 alleviates hepatic fibrogenesis by targeting the miR-92b-3p/Smad7 axis, and they also indicate that circPSD3 may serve as a potential biomarker for HF.

INTRODUCTION

Recent estimates show that 844 million people worldwide have suffered from chronic liver diseases, with 2 million deaths per year.[1] Persistent liver injury secondary to conditions such as viral hepatitis, drug-induced toxicity, nonalcoholic steatohepatitis (NASH), and alcoholic liver disease (ALD) can result in progressive hepatic fibrosis (HF), ultimately leading to hepatic cirrhosis or hepatocellular carcinoma (HCC), even though the early stage of HF is reversible.[2–5] Notably, fibrogenesis is a critical process that results in the formation of a temporary extracellular matrix (ECM)-rich barrier to fight against infection and maintain tissue integrity after self-limiting injury and acute inflammation. However, when liver injury continues or liver repair capacity is impaired, fibrogenesis cannot be reversed, and the deposition of collagen-enriched ECM (e.g., collagen type I alpha 1 chain [COL I] and COL III) is accelerated and leads to the formation of a fibrous scar.[6] Multiple cell types and secreted mediators are involved in the progression of HF. Notably, hepatic stellate cells (HSCs), the key cells responsible for the secretion of ECM proteins, play a vital role in the initiation and progression of HF. In normal liver, HSCs exhibit a quiescent and non-proliferative state and are located in the perisinusoidal space of Disse, functioning in lipid droplet storage.[7] Once induced by liver injury factors or stimuli from the microenvironment, quiescent HSCs are activated. They transdifferentiate to myofibroblasts and promote the expression of α-smooth muscle actin (α-SMA), accompanied by lipid droplet loss and fibroblast phenotype acquisition, which shows high proliferative and contractile characteristics and produces collagen and other ECM constituents.[7] Transforming growth factor (TGF)-β1, a key pro-fibrogenic cytokine, can also drive HSC activation and promote ECM deposition during chronic liver injury, consequently resulting in hepatic fibrogenesis.[8] Although the mechanism of HF development has been investigated, no valid methods or drugs to treat HF are available. Therefore, it is necessary to develop an effective therapeutic strategy for HF and elucidate the mechanism of hepatic fibrogenesis.

Received 15 March 2020; accepted 10 January 2021;
https://doi.org/10.1016/j.omtn.2021.01.007.

[5]These authors contributed equally

Correspondence: Jun Li, Professor of Pharmacology, Inflammation and Immune Mediated Diseases Laboratory of Anhui Province, Anhui Institute of Innovative Drugs, School of Pharmacy, Anhui Medical University, 81 Mei Shan Road, Hefei, Anhui Province 230032, China.
E-mail: lj@ahmu.edu.cn
Correspondence: Cheng Huang, Associate Professor of Pharmacology, Inflammation and Immune Mediated Diseases Laboratory of Anhui Province, Anhui Institute of Innovative Drugs, College of Pharmacy, Anhui Medical University, 81 Mei Shan Road, Hefei, Anhui Province 230032, China.
E-mail: huangcheng@ahmu.edu.cn

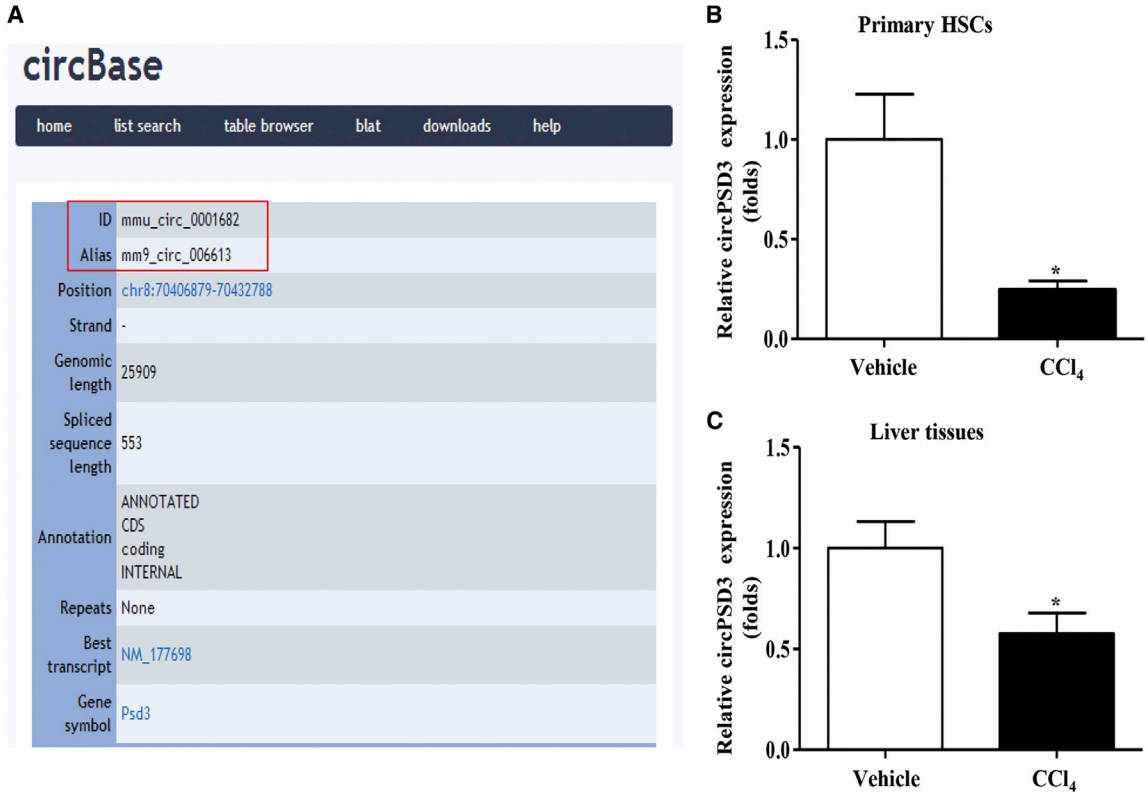

Figure 1. Low expression of circPSD3 in CCl_4-induced mouse HF

(A) ID number and alias of circPSD3 (mmu_circ_0001682/mm9_circ_006613) from the circBase database. (B) The expression of circPSD3 was downregulated in primary HSCs of the CCl_4-induced HF group. (C) The expression of circPSD3 was downregulated in liver tissues of the CCl_4-induced HF group. Quantitative real-time PCR real analyses were used for detecting the expression of circPSD3. *$p < 0.05$ versus vehicle group. Data were expressed as mean ± SEM, n = 6.

Non-coding RNAs, such as microRNAs (miRNAs) and long non-coding RNAs (lncRNAs), are involved in the pathogenesis of HF and can be used as potential biomarkers.[9,10] Circular RNA (circRNA), a novel type of non-coding RNA, has recently gained attention as a biomarker for HF treatment. Fortunately, with the development of next-generation sequencing and bioinformatics, the diagnostic and prognostic potential of circRNA in different diseases has been investigated.[11] Because of the absence of 5′–3′ ends and poly(A) tail, circRNAs are highly stable and more resistant to degradation by exonuclease RNase R compared to linear RNA.[12] Notably, circRNAs are abundant in the eukaryotic transcriptome and conserved between humans and mice.[13,14] Moreover, functional studies confirmed their inexplicable role in different hepatic diseases. For instance, the expression of circMTO1, circHIAT1, and cSMARCA5 is aberrantly reduced in HCC tissues, and forced expression can inhibit the progression of HCC.[15–17] circRNA_0046367 acts as a suppressor in hepatic steatosis.[18] Recently, a microarray study by Zhou et al.[19] reported that the amount of circRNAs changed in carbon tetrachloride (CCl_4)-induced mouse liver fibrosis tissues, and functional studies indicated that mmu_circ_34116 could inhibit HSC activation. In addition, circMTO1 was downregulated during the progression of human HF, and the circMTO1/miR-17-5p/Smad7 axis regulated the activation and proliferation of HSCs.[20] This suggested that circRNAs might play a crucial role in HF development and progression.

Concordantly, our previous study using RNA high-throughput sequencing technology showed that circRNAs were significantly altered in primary HSCs of mice with CCl_4-induced HF and that circFBXW4 possessed anti-fibrotic potential, but there are some circRNAs that have undergone significant changes during the progression of HF whose functions are unknown.[21] In the present study, we aimed to investigate the role of another important circRNA in HF development. First, we found that the expression of mmu_circ_0001682/mm9_circ_006613/circPSD3 (from exons 4–8 of Pleckstrin and Sec7 domain-containing 3 [PSD3] gene locus) was aberrantly reduced in primary HSCs of mice with CCl_4-induced HF compared to that in the oil-treated group, consistent with our sequencing data. Using the UCSC Genome Browser, we identified that hsa_circ_0002111 (circPSD3)—human coordinates from PSD3 gene locus—was consistently downregulated in human HF tissues. Functionally, increases in circPSD3 levels suppressed the activation and proliferation of HSCs and alleviated CCl_4-induced HF, as indicated by reduced fibrotic regions, liver injury index, and pro-inflammatory cytokine secretion. Mechanistically, we found that circPSD3 acted as a miRNA sponge for miR-92b-3p, subsequently

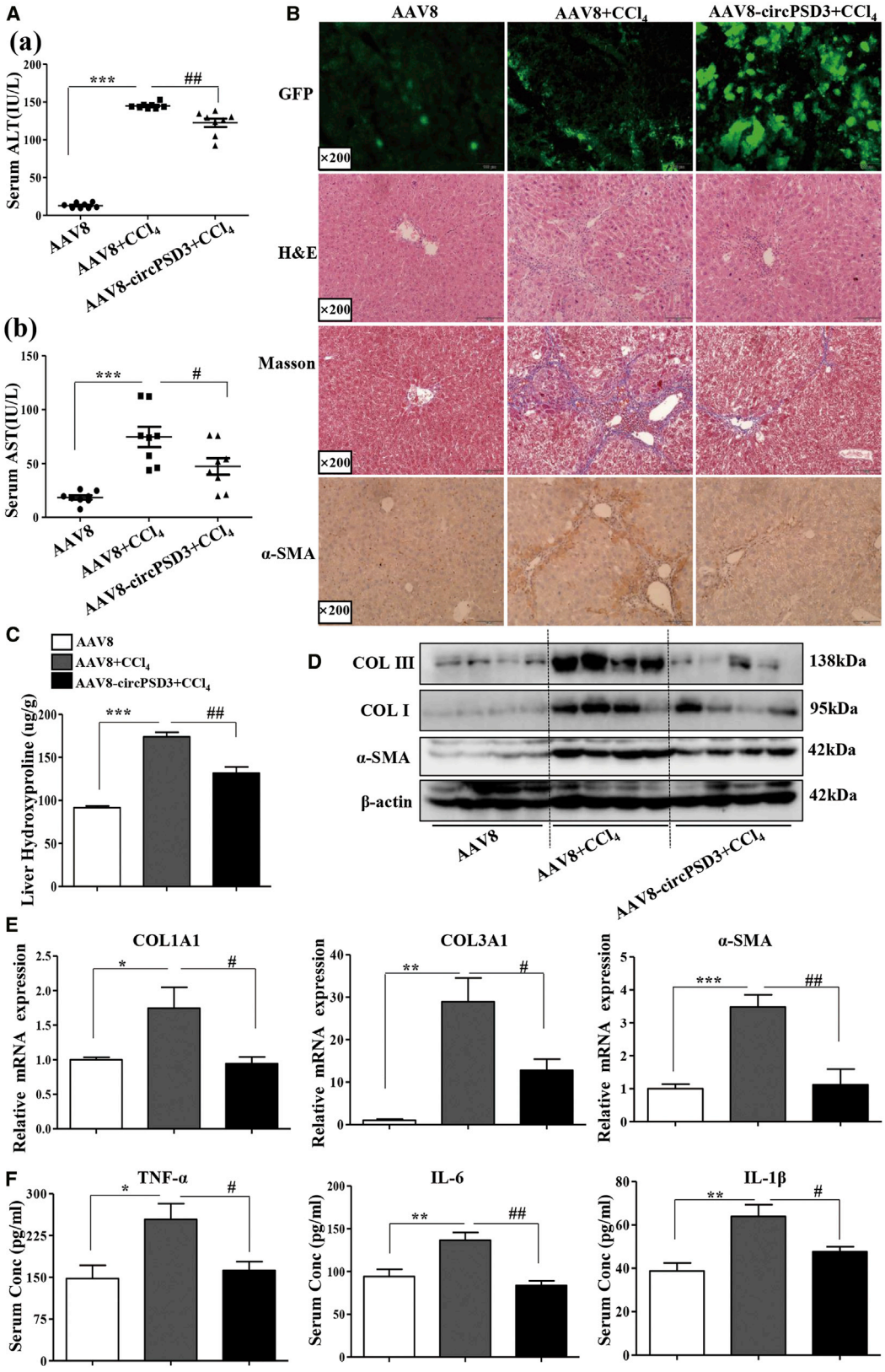

(legend on next page)

regulating the expression of Smad7, suggesting that circPSD3/miR-92b-3p/Smad7 exerted an important role in HSC activation and hepatic fibrogenesis. In conclusion, our present study provides novel insights into the therapeutic potential and regulatory mechanism of circPSD3 in HF. To our knowledge, our study is the first to demonstrate the therapeutic potential of circPSD3 in hepatic fibrogenesis and provide a novel approach for treating HF.

RESULTS

Aberrant decrease in circPSD3 level in mice with CCl_4-induced HF

As previously shown, a significant number of circRNAs were deregulated in primary HSCs of mice with CCl_4-induced HF, and the level of mmu_circ_0001682/mm9_circ_006613, named circPSD3 (from PSD3), markedly decreased in the CCl_4-treated group.[21] To confirm the expression of circPSD3 in HF, we verified successful model establishment. Hematoxylin and eosin (H&E) staining revealed excessive inflammatory cell infiltration, hepatocyte necrosis, and formation of pseudolobules in the CCl_4-treated group (Figure S1A). Masson staining revealed massive deposition of collagen in the liver of CCl_4-treated mice compared to that in the vehicle group (Figure S1A). Moreover, serum ALT and AST levels substantially increased in the CCl_4-treated group (Figure S1B), suggesting a severe injury in HF. At the mRNA and protein level, α-SMA and COL I were significantly upregulated in the fibrosis model group compared to the vehicle group (Figures S1C and S1D). Importantly, the mRNA expression of α-SMA and COL I increased in primary HSCs of the CCl_4-treated group (Figure S1E). These data indicated the successful establishment of a mouse model with CCl_4-induced HF and HSC activation. By using circBase (http://circrna.org/cgi-bin/singlerecord.cgi?id=mmu_circ_0001682), we identified mmu_circ_0001682/mm9_circ_006613/circPSD3 (Figure 1A). To validate the expression of circPSD3, we isolated primary HSCs from two mouse groups. quantitative real-time PCR showed that the expression of circPSD3 was downregulated in primary HSCs of mice with CCl_4-induced HF (Figure 1B). Moreover, circPSD3 was expressed at low levels in the liver tissues of mice with CCl_4-induced HF (Figure 1C). These results suggested that circPSD3 might be a novel regulator of HSC activation and CCl_4-induced HF.

Ectopic expression of circPSD3 alleviated HF *in vivo*

To study the function of circPSD3 in CCl_4-induced HF, the adeno-associated virus serotype 8 (AAV8) vector carrying circPSD3 was utilized. The detailed process for model establishment is shown in Figure S2A. First, we detected the infection efficiency of AAV8-circPSD3 by observing the GFP fluorescence of fresh liver slices in order to confirm the successful delivery of circPSD3 (Figure S2B). qRT-PCR also showed that circPSD3 was overexpressed in the mouse liver (Figure S2C). Serum ALT and AST levels significantly decreased in AAV8-circPSD3-transfected mice compared to the AAV8 empty vector group when challenged with chronic CCl_4 treatment, indicating that high expression of circPSD3 could alleviate CCl_4-induced liver injury (Figure 2A). Compared to the AAV8 empty vector-transfected CCl_4-treated group, the CCl_4-treated group exhibited decreased inflammatory cell infiltration, hepatocyte necrosis, and collagen fiber deposition upon administration of AAV8-circPSD3, as confirmed by H&E and Masson staining (Figure 2B). The α-SMA-positive region also decreased in size in the CCl_4-treated group after transfection with AAV8-circPSD3 (Figure 2B), indicating the repressive effect of circPSD3 on activated HSCs. Moreover, lower hydroxyproline level indirectly revealed a decreased collagen production in the AAV8-circPSD3-transfected CCl_4-treated group compared to the AAV8 empty vector-treated mouse HF group (Figure 2C). At the protein and mRNA level, COL I, COL III, and α-SMA were considerably downregulated in the CCl_4-treated group after transfection with AAV8-circPSD3 (Figures 2D and 2E). Reduced serum tumor necrosis factor (TNF)-α, interleukin (IL)-1β, and IL-6 levels in AAV8-circPSD3-transfected mice suggested a reduction in inflammation after CCl_4 challenge (Figure 2F). Therefore, these results suggested that overexpression of circPSD3 could alleviate CCl_4-induced liver injury, inflammation, and fibrosis.

circPSD3 was downregulated in activated LX-2 cell lines

circPSD3 is derived from PSD3, located on chromosome 8p22. PSD3, also known as HCC-associated antigen 67, is a risk factor for systemic sclerosis with extensive fibrosis of skin and internal organs.[22] Using the UCSC Genome Browser, we found that circPSD3 was conserved in humans (hsa_circ_0002111) and mice (mmu_circ_0001682), with both human and mice circPSD3 originating from 5 exons of PSD3 through back-splicing. Moreover, hsa_circ_0002111 was also included in circBase, as shown in Figure S3A. Sanger sequencing confirmed the circular junction site (Figure 3A). Compared to PSD3 mRNA, circPSD3 was more resistant to digestion by RNase R exonuclease (Figure 3B), suggesting that circPSD3 was relatively more stable than the linear mRNA, making circPSD3 a promising disease marker. Actinomycin D, an inhibitor of transcription, was used to detect the stability of circPSD3. As shown in Figure 3C, total RNA was harvested at the indicated time points (0, 4, 8, 12, and 24 h) after treatment with 2 μg/mL actinomycin D. Quantitative real-time PCR using circPSD3 and PSD3 mRNA indicated that the circRNA isoform was extremely stable, with a transcript half-life >24 h, while the linear transcript PSD3 exhibited

Figure 2. Overexpression of circPSD3 *in vivo* ameliorated CCl_4-induced HF

(A) Serum ALT (a) and AST (b) levels were detected in AAV8 empty vector, AAV8+CCl_4, and AAV8-circPSD3+CCl_4 groups. ALT and AST levels were decreased in the AAV8-circPSD3-treated HF group. (B) Representative efficient transduction of GFP-AAV8-circPSD3 in liver tissue slices. Representative H&E and Masson staining images of liver from three groups and immunohistochemistry of α-SMA. (original magnification, ×200; scale bar, 100). (C) The hydroxyproline content of liver tissues were detected in the three groups. (D and E) The protein and mRNA levels of COL III, COL I, and α-SMA in liver tissues from the three groups were analyzed by western blotting and quantitative real-time PCR. (F) Serum TNF-α, IL-6, and IL-1β levels were determined by ELISA in the three groups. $^{*}p < 0.05$, $^{**}p < 0.01$, $^{***}p < 0.001$ versus the AAV8 empty vector group; $^{\#}p < 0.05$, $^{\#\#}p < 0.01$ versus the AAV8+CCl_4 group. Data represent mean ± SEM, n = 8. AAV8 represents the AAV8 empty vector-treated vehicle group, AAV8+CCl_4 represents the AAV8 empty vector-treated HF group, and AAV8-circPSD3+CCl_4 represents the AAV8-circPSD3-treated HF group.

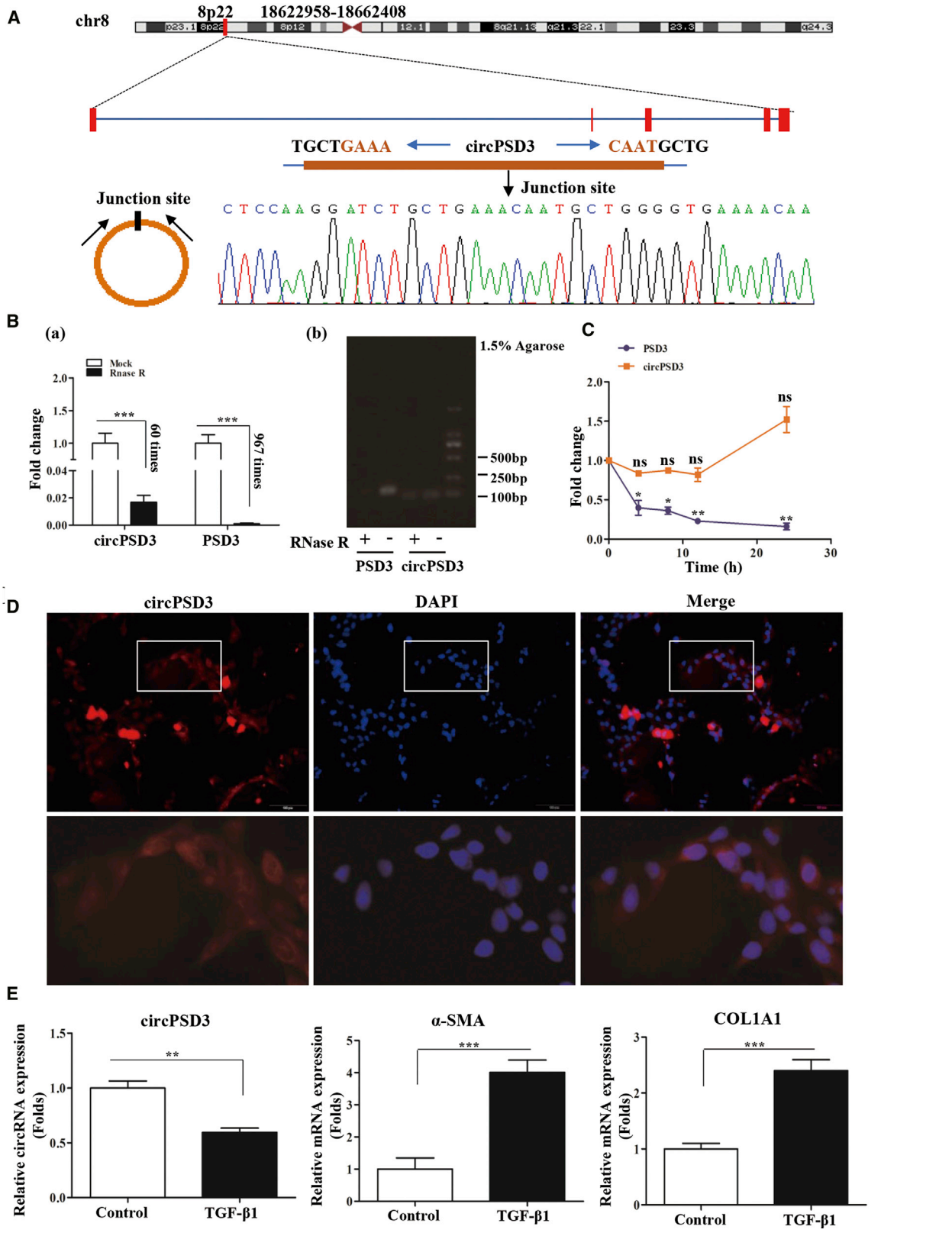

(legend on next page)

half-life <4 h. Fluorescence *in situ* hybridization (FISH) showed that circPSD3 was preferentially localized in the cytoplasm of LX-2 cells (Figure 3D), and weak Cy3 fluorescence of circPSD3 was observed in the TGF-β1 (10 ng/mL)-treated group (Figure S3B), confirming that circPSD3 level decreased in activated HSCs. Quantitative real-time PCR indicated that circPSD3 decreased in LX-2 cells after TGF-β1 treatment (Figure 3E) and that this was accompanied by increased mRNA and protein expression of α-SMA and COL I (Figure 3E; Figure S3C).

Lentivirus (LV)-mediated overexpression of circPSD3 inhibited activation and proliferation of HSCs

To further explore the function of circPSD3, we constructed overexpressing plasmids packaged within lentivirus *in vitro* and transfected LX-2 cells. GFP fluorescence observation and quantitative real-time PCR confirmed that circPSD3 was successfully overexpressed in LX-2 cells (Figures S4A and S4B). For subsequent verification of the circPSD3 function, we used 2 μg/mL puromycin to screen stable cell lines. As shown in Figures 4A and 4B, overexpression of circPSD3 significantly decreased the mRNA and protein expression of α-SMA and COL I, even in the presence of the pro-fibrogenic cytokine TGF-β1, suggesting that circPSD3 can inhibit HSC activation. Cell cycle analysis by flow cytometry showed that cells in the circPSD3-overexpressing group were significantly arrested in the G0/G1 phase compared to the LV-control group ($p < 0.01$) when stimulated by TGF-β1 (Figure 4C), indicating that overexpression of circPSD3 can repress the proliferation of HSCs. In addition, cell counting kit-8 (CCK-8) analyses showed that high expression of circPSD3 could suppress cell viability compared to the LV-control group with TGF-β1 treatment ($p < 0.05$) (Figure 4D). Downregulation of C-Myc and CDK4 proteins in the circPSD3-overexpressing group with TGF-β1 treatment further confirmed that circPSD3 might inhibit the proliferation of HSCs in HF (Figure 4E).

siRNA-mediated silencing of circPSD3 exacerbated activation and proliferation of HSCs

To further clarify the function of circPSD3, we utilized circPSD3 siRNA to inhibit the expression of circPSD3. The silencing efficiency is shown in Figure S4C; the expression levels of circPSD3 were considerably decreased in circPSD3 siRNA (si-circPSD3)-transfected LX-2 cells compared to the siRNA negative control (si-NC) group. As shown in Figure 5A, circPSD3 expression levels were further decreased in TGF-β1-activated LX-2 cells with si-circPSD3 treatment. Notably, enhanced mRNA and protein expression levels of α-SMA and COL I in circPSD3 knockdown cells treated by TGF-β1 suggested that silencing of circPSD3 could promote the activation of LX-2 cells (Figures 5A and 5B). Cell cycle analysis by flow cytometry showed that LX-2 cells in G0/G1 phase were significantly reduced ($p < 0.01$) and cells in G2 phase were significantly increased ($p < 0.05$) in the circPSD3 knockdown group with TGF-β1 treatment (Figure 5C), indicating that circPSD3 silencing could accelerate the proliferation of HSCs. In addition, CCK-8 analyses showed that knockdown of circPSD3 could boost the cell viability of LX-2 cells (Figure 5D). Enhanced expression of C-Myc and CDK4 further indicated that lower expression of circPSD3 could enhance the proliferation of HSCs (Figure 5E). Collectively, loss-of-function and gain-of-function analyses *in vitro* suggested circPSD3 may restrain the activation and proliferation of HSCs in HF.

circPSD3 inhibited activation and proliferation of HSCs by regulating the miR-92b-3p/Smad7 axis

Cytoplasmic exon circRNAs often act as miRNA sponges. Given that circPSD3 was an exonic circRNA and mostly located in the cytoplasm (Figure 3D), we investigated whether circPSD3 could act as a miRNA sponge. Using miRNA sequencing, we found that miRNAs differentially changed in LX-2 cells transfected with LV-circPSD3 (Figure 6A). Importantly, miR-92b-3p was markedly downregulated in the circPSD3-overexpressing group compared to the LV-control group (Figure 6B). miR-92b-3p is abnormally upregulated in HCC tissues and functions as a tumor promoter.[23] Moreover, the Starbase software prediction (http://starbase.sysu.edu.cn/agoClipRNA.php?source=circRNA&flag=none&clade=mammal&genome=human&assembly=hg19&miRNA=hsa-miR-92b-3p&clipNum=1&deNum=0&target=hsa_circ_0002111) indicates that miR-92b-3p harbors an ideal target site for circPSD3. To confirm the binding between miR-92b-3p and circPSD3, we performed dual luciferase reporter assay using wild-type (WT) and mutant circPSD3 (the predicted miR-92b-3p-binding site was mutated). As shown in Figure 6C, the luciferase activity markedly declined when 293T cells were co-transfected with miR-92b-3p mimics and circPSD3-WT compared to when co-transfected with miR-92b-3p-NC. When co-transfected with circPSD3-mu, miR-92b-3p failed to downregulate the luciferase activity, indicating that the mutant site was constructed successfully. Given the unknown function of miR-92b-3p in HF, we explored its effect *in vitro*. As shown in Figure S4A, miR-92b-3p levels increased significantly in LX-2 cells activated by TGF-β1. We overexpressed the miRNA by using miR-92b-3p mimics. As shown in Figure S4B, miR-92b-3p was successfully overexpressed. As expected, enhancement of miR-92b-3p promoted the mRNA and protein expression of α-SMA and COL I (Figures S4C and S4E), suggesting the promotive HSC activation role of

Figure 3. Lower abundance of circPSD3 in activated LX-2 cell lines

(A) Schematic illustration indicating the circularization of 5 exons of PSD3, forming circPSD3. Sanger sequencing analysis confirmed the circular sites of circPSD3. The arrow represents the "head-to-tail" splicing site. (B) circPSD3 and linear PSD3 levels in LX-2 cells were determined by qRT-PCR after treatment with RNase R for 30 min, and the products were detected by 1.5% agarose gel electrophoresis. circPSD3 was more stable than linear PSD3 (1,000 times digestion than mock group). ***$p < 0.001$ versus mock group. (C) circPSD3 and linear PSD3 levels in LX-2 cells were determined by quantitative real-time PCR after treatment with actinomycin D at different time points (0, 4, 8, 12, 24 h). *$p < 0.05$, **$p < 0.01$ versus 0 h. ns, no statistical significance. (D) RNA FISH for circPSD3 was detected in LX-2 cells. Cy3-labeled circPSD3 appeared red, and nuclei were stained with 2-(4-Amidinophenyl)-6-indolecarbamidine dihydrochloride (DAPI,blue). Scale bar, 100 μm. (E) circPSD3, α-SMA, and COL I expression levels in TGF-β1 (10 ng/mL)-treated LX-2 cells were determined by quantitative real-time PCR . **$p < 0.01$, ***$p < 0.001$ versus normal control group. Data were expressed as mean ± SEM, with three independent experiments calculated.

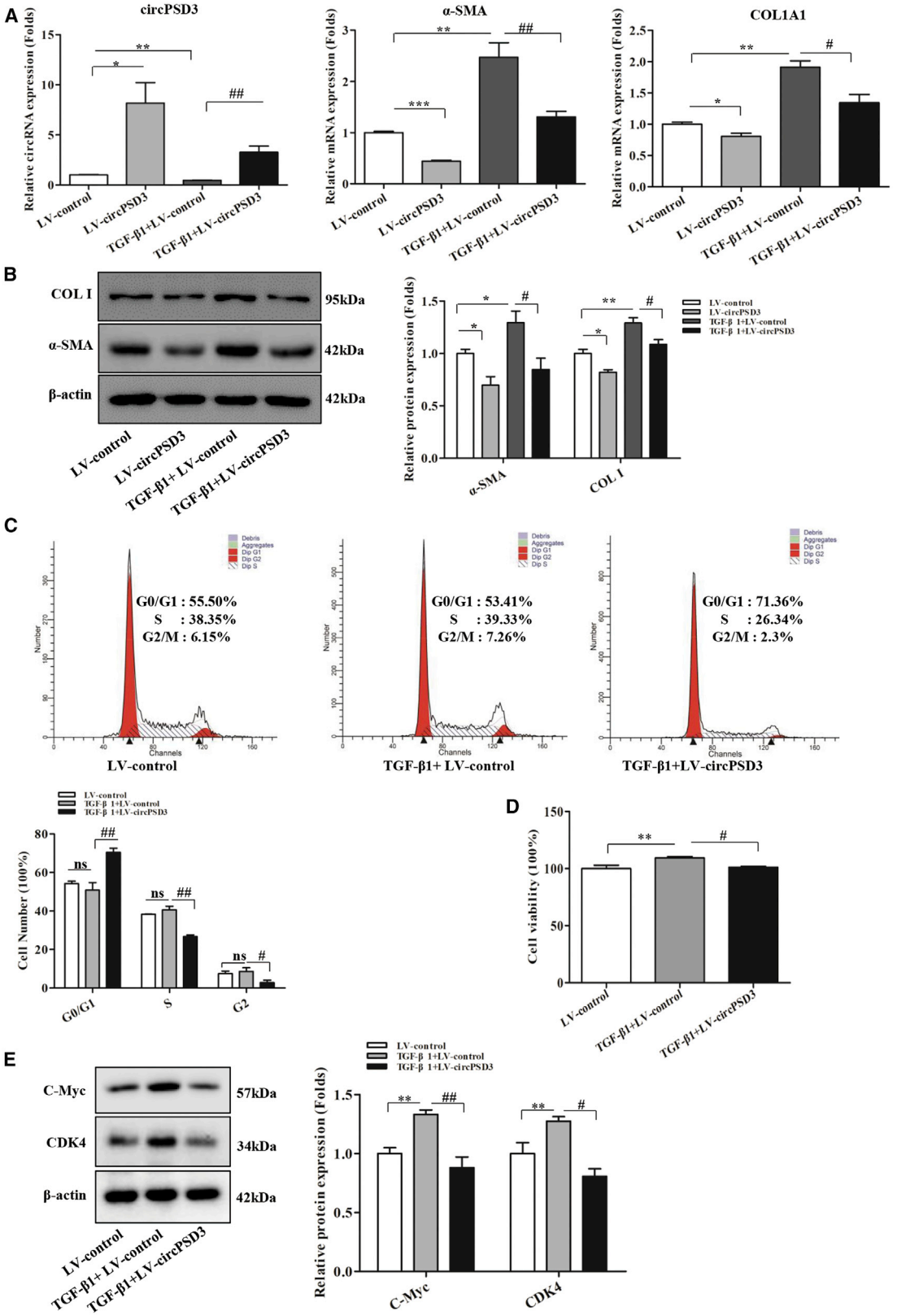

(legend on next page)

miR-92b-3p. Interestingly, a high level of miR-92b-3p could inhibit the mRNA and protein production of Smad7 (Figures S4D and S4E). Smad7 is a negative regulator of the TGF-β1/Smad signaling pathway in HF.[24] Moreover, the binding between miR-92 and Smad7 has been already confirmed in HCC.[23] Therefore, we were interested in the role of the circPSD3/miR-92b-3p/Smad7 axis in the activation and proliferation of HSCs in HF. As shown in Figures 6D and 6E, ectopic expression of circPSD3 could promote the mRNA and protein expression of Smad7, whereas miR-92b-3p significantly reversed the effect. In addition, miR-92b-3p could eliminate the suppressive activation and proliferation effect of circPSD3 on HSCs. As shown in Figures 6F and 6G, high expression of circPSD3 could downregulate the expression of α-SMA and COL I at mRNA and protein levels, while treatment with miR-92b-3p mimics in this background could evidently restore their expression compared to miR-92b-3p mimic NC-treated circPSD3-overexpressing cells. As shown in Figure 6H, the protein levels of C-Myc and CDK4 were restored when circPSD3-overexpressing cells were treated by miR-92b-3p mimics. Moreover, the cell viability was increased in the LV-circPSD3 group with miR-92b-3p mimic treatment (Figure 6I). These results indicated that circPSD3 might repress the activation and proliferation of HSCs by regulating the miR-92b-3p/Smad7 axis.

Low expression of circPSD3 in human HF

We investigated whether circPSD3 was functionally involved in human HF by regulating the expression of miR-92b-3p and Smad7. In addition to an abnormal deposition of ECMs and α-SMA-positive regions (Figure 7A), we observed a remarkable downregulation in circPSD3 in liver tissues of the fibrosis patient group (Figure 7B). Subsequently, we detected an abundance of miR-92b-3p and Smad7 in these patients. Interestingly, we found that miR-92b-3p was abnormally upregulated, with a lower expression of Smad7 in the fibrosis group compared to the normal group (Figures 7C, 7D, and 7F). Importantly, we found that the level of miR-92b-3p gradually declined with the increase in circPSD3 expression (Figure 7E). These results confirmed that the repressive effect of circPSD3 was subject to the presence of the sponge miR-92b-3p in HF.

DISCUSSION

HF is detrimental to human health, and given the complexity of its pathogenesis, no effective diagnosis or standard treatment is available so far. In recent decades, many reports highlighted the role of non-coding RNAs such as miRNAs and lncRNAs in hepatic fibrogenesis. For example, high levels of miR-378-3p and miR-185 inhibit the activation of HSCs by regulating targeted mRNA expression, ameliorating hepatic fibrogenesis.[25,26] In our previous study, we demonstrated that the lncRNA HOTAIR promoted the activation of HSCs in hepatic fibrogenesis.[27] However, the role of circRNAs, a class of abundant and conserved non-coding RNA in animals, in HF remains largely unknown.[14] Thanks to the rapid development of RNA sequencing and bioinformatics, important roles of circRNAs in many cancers, including gastric, breast, and liver cancers, have been elucidated.[17,28,29] Recent studies have described the role of circRNAs in organ fibrosis. For instance, circRNA-010567 aggravates cardiac fibrosis via sponging of miR-141, an anti-fibrotic factor.[30] Zhou et al.[31] found that low expression of circHECTD1 could lead to the increased HECTD1 mRNA expression through a pre-mRNA competition mechanism, thereby regulating the activation of macrophages in silicosis, a disease closely related to lung fibrosis. Importantly, several studies indicated a vital role of circRNA in HF. The expression of many circRNAs changed in tissues with CCl_4-induced HF.[19] Moreover, Wang et al.[20] showed that circMTO1 could repress liver fibrogenesis by sponging miR-17-5p, thereby regulating Smad7 expression. In our present study, we found that circPSD3 was expressed at abnormally low levels in primary HSCs of mice with CCl_4-induced HF, consistent with our previous results.[21] Overexpression of circPSD3 via an AAV8-mediated gene delivery system in mice significantly alleviated CCl_4-induced liver damage, cytokine-mediated inflammation, collagen deposition, and α-SMA-positive region. Given the role of activated HSCs in hepatic fibrogenesis, we suspected that circPSD3 might play a crucial role in activation and proliferation of HSCs, thereby regulating hepatic fibrogenesis.

circRNAs are abundant, stable, and conserved between species. Circularization of transcribed exons and inverted repeats within long flanking introns results in the generation of conserved circRNAs in human and mouse fibroblasts.[13] This conservation makes circRNAs potential markers for disease prediction. circPSD3 was conserved between mouse (mmu_circ_0001682) and human (hsa_circ_0002111) based on UCSC Genome Browser prediction. We also found that circPSD3 was abundant in quiescent LX-2 cells and predominantly located in the cytoplasm. Moreover, circPSD3 level decreased when LX-2 cells were challenged with 10 ng/mL TGF-β1. Overexpression of circPSD3 restrained the production of α-SMA and COL I. Furthermore, a high level of circPSD3 inhibited further activation of LX-2 cells in the G0/G1 phase and inhibited the expression of proliferation-related proteins C-Myc and CDK4. These findings indicated that circPSD3 might function as a novel regulator of HSC activation and proliferation in HF. However, its mechanism of action is still unclear.

Studies showed that cytoplasmic exon circRNAs mainly functioned through a miRNA sponge mechanism.[32] Intriguingly, a study in

Figure 4. Overexpression of circPSD3 *in vitro* repressed the activation and proliferation of LX-2 cells

(A) Overexpression of circPSD3 inhibited the mRNA expression levels of α-SMA and COL1A1. circPSD3, α-SMA, and COL1A1 expression levels were analyzed by quantitative real-time PCR. (B) Enhancement of circPSD3 repressed the protein expression levels of α-SMA and COL I. α-SMA and COL I were analyzed by western blotting. (C) Flow cytometry showed the cell cycle distribution in G0/G1 phase increased in circPSD3-overexpressing cells with TGF-β1 treatment. (D) Effect of circPSD3 overexpression on LX-2 cell viability detected by CCK-8 assays at 24 h TGF-β1 treatment (n = 6). (E) Effect of circPSD3 overexpression on proliferation-associated protein expression. c-Myc and CDK4 protein levels in circPSD3-overexpressing LX-2 cells with TGF-β1 treatment were determined and analyzed by western blotting. $^{*}p < 0.05$, $^{**}p < 0.01$, $^{***}p < 0.001$ versus LV-control; $^{\#}p < 0.05$, $^{\#\#}p < 0.01$ versus LV-control cells with TGF-β1 treatment. Data were expressed as mean ± SEM, with three independent experiments calculated.

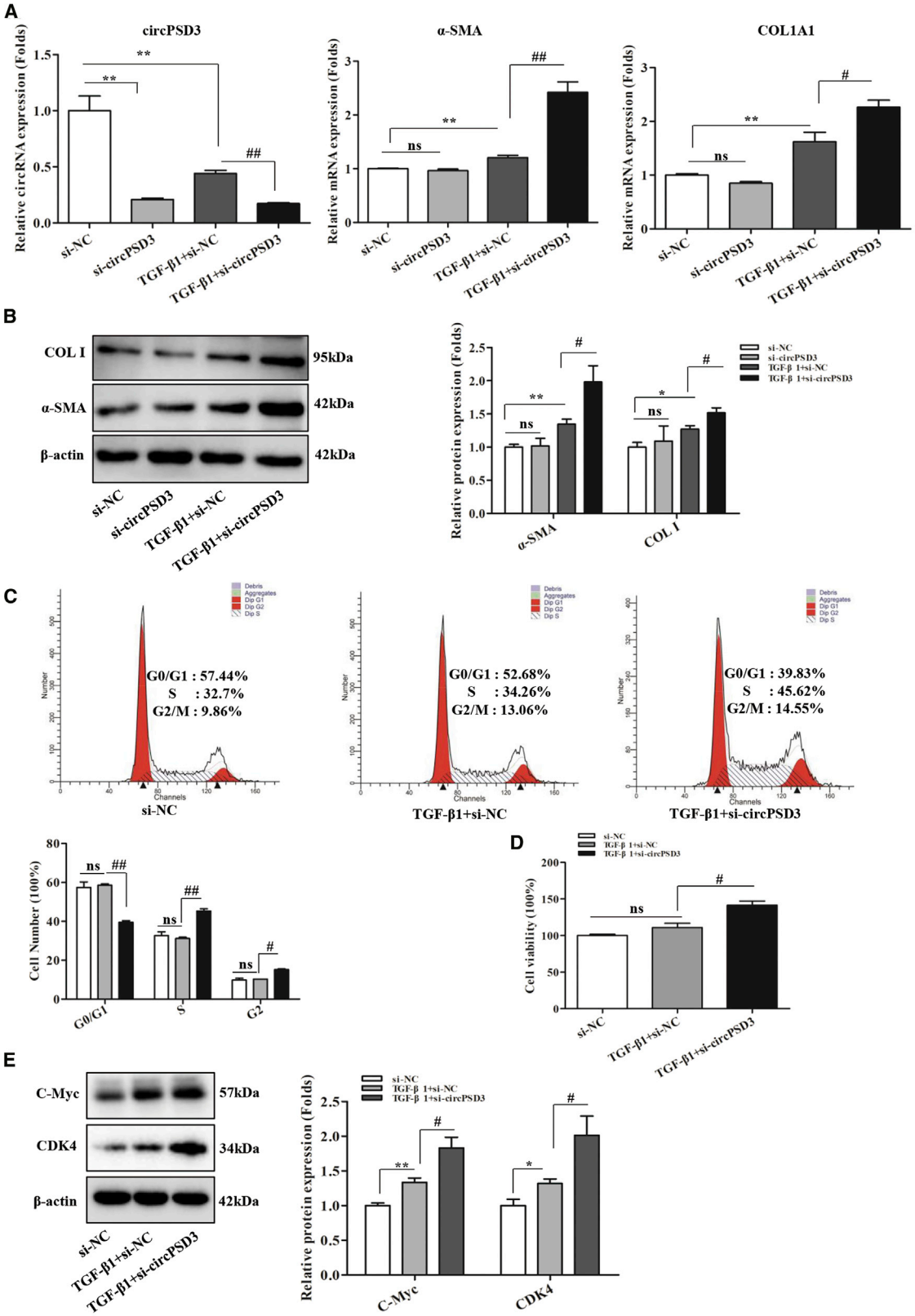

(legend on next page)

2013 showed that CDR1as, a human circRNA, had 63 conserved binding sites for miR-7 and acted as a sponge of miR-7 in neuronal tissues.[33] Many circRNAs were identified as sponges for different miRNAs involved in various biological and pathological processes.[11,34] miRNA sequencing revealed that the expression of a variety of miRNAs changed in circPSD3-overexpressing LX-2 cells. Of note, the expression of miR-92b-3p decreased sharply in the overexpressed group; further, Starbase website prediction revealed that miR-92b-3p harbored potential binding sites for circPSD3. Zhuang et al.[23] reported that miR-92b promoted cell proliferation and metastasis by inhibiting the expression of Smad7 in HCC, but whether miR-92b was involved in HF remained largely unknown. Interestingly, we observed a negative correlation between circPSD3 and miR-92b-3p in human HF tissues. We found that miR-92b-3p was abnormally upregulated in LX-2 cells treated with TGF-β1. Ectopic expression of miR-92b-3p by miRNA mimics could enhance the production of α-SMA and COL I but reduce the expression of Smad7. Furthermore, overexpression of miR-92b-3p impaired the inhibitory effect of circPSD3 on LX-2 cell activation and proliferation and compromised the promotive effect of circPSD3 on Smad7.

Thus, circPSD3 may hinder the activation and proliferation of HSCs in hepatic fibrogenesis by regulating the miR-92b-3p/Smad7 axis (Figure 8). Nevertheless, whether circPSD3 exists in exosomes is not clear, and the role played by nuclear circPSD3 is still unclear. Further studies are necessary to unravel the mechanism of action of circPSD3. The parental gene of circPSD3, PSD3, has been reported to be a risk factor in systemic sclerosis.[22] However, the role of PSD3 in HF is unknown. In the future, we will explore the function and mechanism of PSD3 in HF and try to elucidate its link with circPSD3.

MATERIALS AND METHODS

Human liver tissues

A total of ten HF tissues associated with HCC and eight normal liver tissues with hepatic hemangioma resection were obtained from the first affiliated hospital of Anhui Medical University (Hefei, China). HF tissues were confirmed by professional pathologists. All tissues were collected immediately after surgical removal from the body. Some tissues were fixed in 4% paraformaldehyde, and the remaining tissues were snap-frozen in liquid nitrogen before storage at −80°C. The present study was approved by the Biomedical Ethics Committee of Anhui Medical University, and all patients provided informed consent. The characteristics of the subjects enrolled in the study for detecting liver circPSD3 expression levels are shown in Table S1.

Animal models

C57BL/6 male mice (6–8 weeks old) were purchased from Anhui Medical University, and all animal experiments were approved by the Animal Care and Use Committee of Anhui Medical University (Hefei, China). HF was induced using intraperitoneal injection of 10% CCl_4 (CCl_4:olive oil = 1:9; dose, 0.001 mL/g/mouse biweekly for 6 weeks). Mice in the vehicle group were injected with the same volume of olive oil for the same time. AAV8-circPSD3 (1.4×10^{12} TU [transducing units] /mL) and AAV8 (Hanbio, Shanghai, China) were intravenously delivered through the tail (100 μL per mouse). One week after viral transduction, mice were injected with 10% CCl_4 or an equal amount of olive oil. Six weeks later, all mice were anesthetized using 5% isoflurane in room air. The blood and liver tissues were collected for further experiments.

Isolation of primary HSCs

The isolation of mouse primary HSCs was performed as previously described.[35] Briefly, liver tissues were digested with mixed digestion liquid (collagenase IV [Sigma-Aldrich, St. Louis, MO, USA] and pronase E [Sigma-Aldrich]). Density gradient centrifugation of dispersed cell suspension was performed using Nycodenz medium (Sigma-Aldrich) dissolved in Gey's Balanced Salt Solution (GBSS) buffer, according to the manufacturer's protocol.

Serum ALT and AST detection

The serum was isolated from whole blood and immediately tested for AST (aspartate aminotransferase) and ALT(alanine aminotransferase). AST/ALT assay kits (Jiancheng Bioengineering Institute, Nanjing, China) were used.

Serum inflammatory cytokine detection

Serum TNF-α, IL-1β, and IL-6 cytokine levels were measured using an ELISA kit (Jiyinmei Biotechnology, Wuhan, China), according to the instruction manual.

Liver hydroxyproline detection

Hydroxyproline assay kit (Jiancheng Bioengineering Institute) was used to detect the hydroxyproline level in each liver tissue. The prepared tissue supernatant was detected at 550 nm.

Histopathology and immunohistochemistry (IHC)

Liver tissues collected from patients and mice were fixed with 4% paraformaldehyde for 24 h, waxed, and sectioned at 5 μm. The sections were used for H&E and Masson staining. IHC of α-SMA (1:200) was performed as previously described.[35]

Figure 5. circPSD3 knockdown exacerbated the activation and proliferation of LX-2 cells

(A) Inhibition of circPSD3 promoted the mRNA expression levels of α-SMA and COL1A1. circPSD3, α-SMA, and COL1A1 expression levels were analyzed by quantitative real-time PCR. (B) Inhibition of circPSD3 promoted the protein expression levels of α-SMA and COL I. α-SMA and COL I were analyzed by western blotting. (C) Flow cytometry showed the cell cycle distribution in G0/G1 phase decreased in si-circPSD3-transfected LX-2 cells with TGF-β1 treatment. (D) Knockdown of circPSD3 promoted the cell viability. Effect of circPSD3 siRNA on cell viability detected by CCK-8 assays. (E) Effect of circPSD3 knockdown on proliferation-associated protein expression. c-Myc and CDK4 protein levels in circPSD3 siRNA-transfected LX-2 cells with TGF-β1 treatment were determined and analyzed by western blotting. $^{*}p < 0.05$, $^{**}p < 0.01$ versus si-NC; $^{\#}p < 0.05$, $^{\#\#}p < 0.01$ versus TGF-β1-treated si-NC cells. Data were expressed as mean ± SEM, with three independent experiments calculated. si-circPSD3 represents circPSD3 siRNA, and si-NC represents negative control.

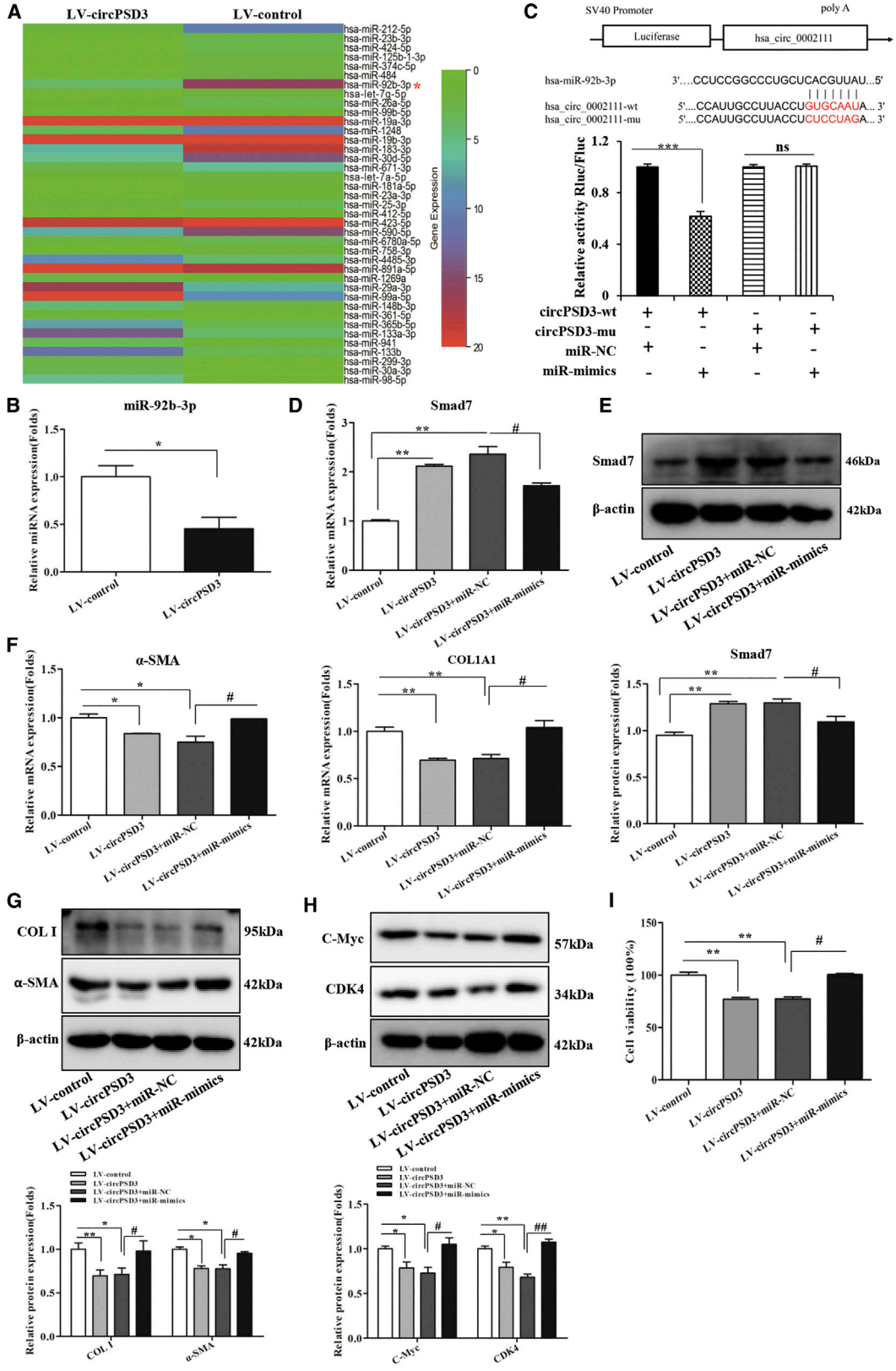

(legend on next page)

Cell culture

LX-2 cells, the human HSCs, were obtained from Procell Life Science & Technology (Wuhan, China) with hort Tandem Repeats STR verification. LX-2 cells were routinely maintained in Dulbecco's modified Eagle's medium (DMEM) supplemented with 100 U/mL penicillin, 100 mg/mL streptomycin (Beyotime, Shanghai, China), and 10% fetal bovine serum (Gibco, CA, USA) at 37°C in an atmosphere of 5% CO_2. Recombinant human TGF-β1 (PeproTech, NJ, USA) was used to activate LX-2 cells.

RNase R and actinomycin D treatment assay

RNase R treatment assay is a common method to verify the stability of circRNAs.[36] Briefly, 2 μg of total RNA was incubated with RNase R (Epicenter Technologies, Madison, WI, USA) for 30 min at 37°C. For the RNase R treatment group, 0.3 μL RNase R (20 U/μL) and 0.6 μL 10× reaction buffer were added. For the mock group, 0.3 μL DEPC-treated water and 0.6 μL 10× reaction buffer were added. Transcription blocking assay was performed by the addition of 2 μg/mL actinomycin D (MedChemExpress, NJ, USA) for 4 h, 8 h, 12 h, and 24 h, and DMSO (Sigma) was used as a control for the cell culture medium. To detect the expression level of circPSD3 and PSD3, the same amount of RNA was utilized for reverse transcription and quantitative real-time PCR analysis.

FISH

Hybridization was performed overnight at 37°C using the circPSD3 probe (Genepharma, Shanghai, China). The sequence of the circPSD3 probe for FISH was 5′-CCAGCATTGTTTCAGCAGATCCTTG-3′. FISH was performed as per the FISH kit instructions (Genepharma). Specimens were observed using an OLYMPUS inverted fluorescence microscope.

Stable cell line establishment

circPSD3 was packaged using lentivirus-GFP-puromycin, which was designed and synthesized by Hanbio. In brief, well-conditioned cells were seeded in 6-well plates at a density of 1×10^5/mL. Lentiviral construct was transfected after cell confluence reached 50%–70%. After the cells were attached to the plates on the second day, the culture medium was discarded, and 1 mL fresh culture medium containing 8 μg/mL polybrene (Hanbio) was added for 30 min at 37°C in 5% CO_2. Then, 40 μL (3×10^8 TU/mL) lentivirus was added to the culture medium for 48 h. The GFP expression efficiency was observed under an inverted fluorescent microscope. For the virus carrying the puromycin resistance gene, fresh culture medium containing 2 μg/mL puromycin was used to screen the stable strains.

siRNA and miRNA mimic transfection

siRNA transfection was carried out as previously described.[35] The sequences of si-circPSD3 and miR-92b-3p mimics were as follows: si-circPSD3, sense 5′-GGAUCUGCUGAAACAAUGCTT-3′ and antisense 5′-GCAUUGUUUCAGCAGAUCCTT-3′; miR-92b-3p mimics, sense 5′-UAUUGCACUCGUCCCGGCCUCC-3′ and anti-sense 5′-AGGCCGGGACGAGUGCAAUAUU-3′; si-NC and miRNA-NC, sense 5′-UUCUCCGAACGUGUCACGUTT-3′ and antisense 5′-ACGUGACACGUUCGGAGAATT-3′. LX-2 cells were seeded into 6-well plates for 24 h and transfected with si-circPSD3 or miR-92b-3p mimics with Lipofectamine 2000 (Invitrogen, Carlsbad, CA, USA); si-NC or miRNA-NC were used as control. Briefly, the equivoluminal Lipofectamine 2000 and si-circPSD3 or miR-92b-3p mimics were separately diluted in Opti-MEM (Gibco) and mixed for 5 min at room temperature (RT). Then, the diluted si-circPSD3 or miR-92b-3p mimics were mixed with the diluted Lipofectamine 2000 and incubated for 20 min at RT. Next, the mixture was applied to LX-2 cells and incubated for 6 h at 37°C in 5% CO_2. After 6 h, the supernatant was replaced by fresh DMEM (10% fetal bovine serum [FBS]) for further study. Total RNA was extracted using TRIzol reagent, and qRT-PCR was performed to verify the gene silencing or mimic efficacy.

Cell cycle analysis

Cell cycle analysis kit (Beyotime) was used for cell cycle analysis. Briefly, collected LX-2 cells were washed for twice by pre-cooling PBS. Then, the cells were fixed in 70% ethanol at 4°C overnight, and PBS was used for washing the fixed cells. Next, the washed cells were stained with 500 μL propidium iodide (PI) staining buffer at 37°C for 30 min in the dark. Flow cytometric analysis was performed on a BD LSR (BD Biosciences, NJ, USA). Cell populations in different phases were quantified by the ModFit data analysis software package (Verity Software House, ME, USA). The experiments were performed in triplicate, and the results of three biological replicates were analyzed statistically.

Figure 6. circPSD3 inhibited activation and proliferation of HSCs via regulating miR-92b-3p/Smad7 axis

(A) Heatmap of differential miRNAs in LV-circPSD3 treated group and LV-control group. Each row represents relative expression levels of a single miRNA, and each column represents an independent sample. The color indicates expression level: red is high and green is low. (B) The expression levels of miR-92b-3p decreased in circPSD3-overexpressing LX-2 cells, and quantitative real-time PCR was used for analysis. *$p < 0.05$ versus LV-control group. (C) Schematic of miR-92b-3p sites in circPSD3 based on complementary sequences. Relative luciferase activity of circPSD3-WT or circPSD3-mutant (mut) were detected in HEK-293T cells after co-transfection with miR-92b-3p mimics or miR-NC. ***$p < 0.001$ versus circPSD3-WT cotransfected miR-mimics. Data were expressed as mean ± SEM with three independent experiments calculated. (D and E) The mRNA and protein expression levels of Smad7 were detected in circPSD3-overexpressing LX-2 cells with miR-NC and miR-92b-3p mimic treatment by quantitative real-time PCR and western blotting. (F and G) The mRNA and protein expression levels of α-SMA and COL I were detected in circPSD3-overexpressing LX-2 cells with miR-NC and miR-92b-3p mimic treatment by quantitative real-time PCR and western blotting. (H) The protein expression levels of C-Myc and CDK4 were detected in circPSD3-overexpressing LX-2 cells with miR-NC and miR-92b-3p mimic treatment by western blotting. (I) Effect of miR-92b-3p mimics on cell viability in circPSD3-overexpressing LX-2 cells at 48 h by performing CCK-8 assays (n = 6). *$p < 0.05$, **$p < 0.01$ versus LV-control group; $^{\#}p < 0.05$, $^{\#\#}p < 0.01$ versus LV-circPSD3+miR-NC group. Data were expressed as mean ± SEM, with three independent experiments calculated. miR-mimics represent miR-92b-3p mimics, and miR-NC represents miR-92b-3p mimics negative control.

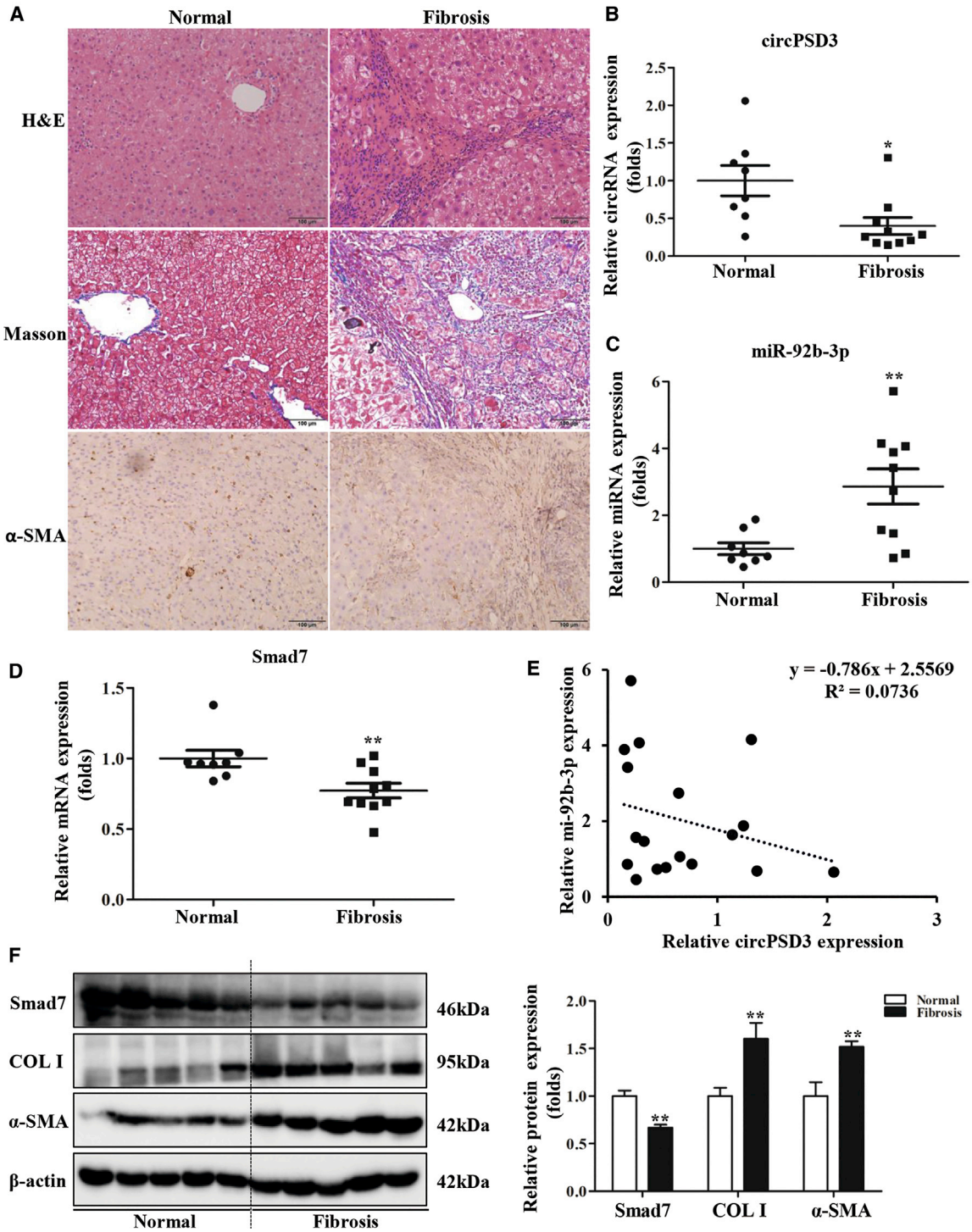

Figure 7. Decreased expression of circPSD3 in human HF

(A) Representative H&E, Masson staining, and immunohistochemistry of α-SMA images from normal liver and HF groups (original magnification × 200 ; scale bar, 100). (B) The expression of circPSD3 was significantly decreased in the HF group, and quantitative real-time PCR was used for analysis. (C) miR-92b-3p expression levels in normal and HF groups were determined by qRT-PCR, and the levels of miR-92b-3p were upregulated in the HF group. (D) The mRNA expression of Smad7 was significantly downregulated in the HF group, and quantitative real-time PCR was used for analysis. (E) The negative relation between circPSD3 and miR-92b-3p in 18 subjects. (F) The protein expression of Smad7, α-SMA, and COL I was determined by western blotting in normal and HF groups. *$p < 0.05$, **$p < 0.01$ versus normal group. Data were expressed as mean ± SEM, with three independent experiments calculated.

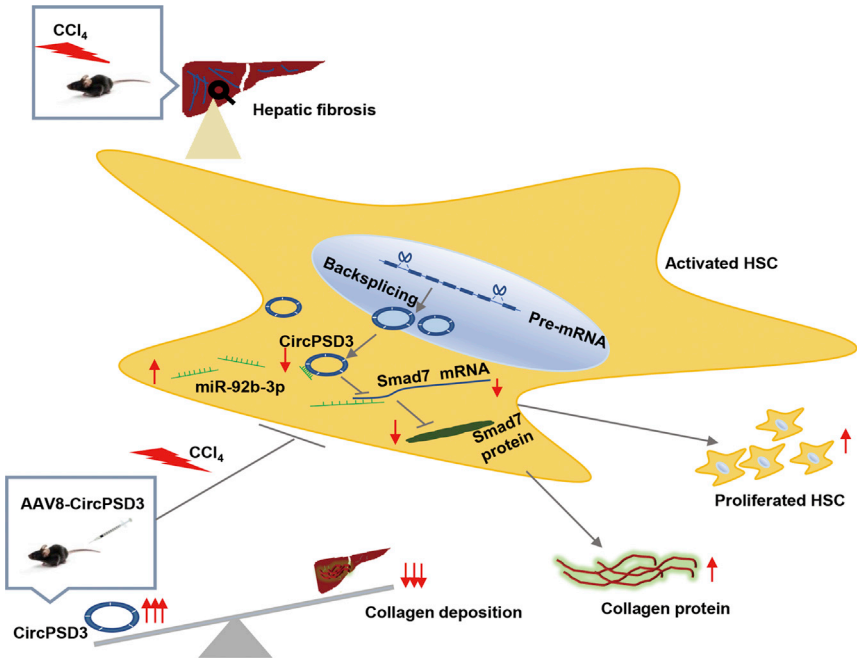

Figure 8. A schematic model of circPSD3 in HF
In respond to chronic injury factors, such as CCl_4, quiescent HSCs were activated and circPSD3 expression levels were decreased. Enhanced expression of circPSD3 could decease CCl_4-induced collagen deposition in mouse liver. Conclusively, circPSD3 may suppress HSC activation and proliferation by sponging miR-92b-3p, thereby promoting expression of Smad7.

CCK-8 assay

Healthy LX-2 cells were seeded into 96-well plates. After transfection with siRNA or lentiviral vector, cells were treated with 10 ng/mL TGF-β1 (Peprotech). After 24 h or 48 h, 10 μL CCK-8 reagent was added to each well. The optical density (OD) was determined using a microplate reader (Molecular Devices, CA, USA) at 450 nm wavelength. All experiments were performed in triplicate and repeated at least three times.

Western blotting

Western blotting was performed as previously described.[35] Liver tissue and LX-2 cell proteins were extracted using RIPA (Radio Immunoprecipitation Assay) lysis buffer (Beyotime) and quantified using the BCA protein assay kit (Beyotime). Rabbit polyclonal anti-COL I, anti-COL III, and anti-Smad7; mouse polyclonal anti-SMA (Bioss, Beijing, China); mouse anti-β-actin (ZSGB-BIO, Beijing, China); and rabbit polyclonal anti-C-Myc and anti-CDK4 (Abcam, Cambridge, UK) were used.

Total RNA extraction and quantitative real-time PCR

Total RNA was extracted from primary HSCs, liver tissues, and LX-2 cells using TRIzol reagent (Invitrogen). Total RNA quantification was performed using Nanodrop 2000 (Thermo Fisher Scientific, MA, USA). First-strand cDNA synthesis and amplification were performed using PrimeScript RT Master Mix (Takara, Japan). Quantitative real-time PCR was performed on the Bio-Rad CFX96 Real-Time PCR system using SYBR-Green (Takara). Mouse GAPDH and human β-actin were used as internal control genes. For miR-92b-3p detection, the procedure was performed according to the manufacturer's instructions of the One-step miRNA qPCR Detection Kit (Biomics, Nantong, Jiangsu, China), and U6 was used as the endogenous control. The fold-change of mRNA or miRNA relative to GAPDH, β-actin, or U6 was determined using the formula $2^{-\Delta\Delta Ct}$. All experiments were performed in triplicate and repeated at least three times. Primer sequences are listed in Table S2.

miRNA-seq

miRNA-seq was performed at Shanghai OG Company (Ao-Ji Biotech, Shanghai, China). Briefly, total RNA of the LV-control group and the LV-circPSD3 group was extracted from LX-2 cells using the mirVana miRNA isolation kit (Thermo Fisher Scientific). The concentration and purity of total RNA were measured using Nanodrop 2000. RNA integrity was assessed using Agilent 2100 Bioanalyzer (Agilent Technologies, CA, USA). A small RNA (sRNA, ~21 nt) library was generated using the NEBNext Multiplex Small RNA Library Prep Set for Illumina (Set 2, New England BioLabs, USA), according to the manufacturer's protocols. After quality control using an Agilent 2100 Bioanalyzer and Qubit 2.0 fluorometer (Invitrogen), sRNA-seq was performed on the HiSeq 2000 Sequencing System (Illumina, San Diego, CA, USA).

Luciferase reporter assay

Healthy 293T cells were seeded into 96-well plates. When the cell density reached 50%–70%, dual-luciferase reporter plasmids and miRNA mimics or NC were co-transfected using LipoFiter 3.0 Transfection reagent (Hanbio). After 48 h incubation, firefly and Renilla luciferase activities were detected on the Dual-Luciferase Reporter Assay system (Promega, Madison, Wisconsin, USA), according to the manufacturer's instructions.

Conservation prediction

circPSD3 chromosome location was determined in mice and humans using the UCSC Genome Browser. The corresponding circRNAs were searched based on the human chromosome location information after transformation. BLAST confirmed the cDNA sequence homology of circRNA in humans and mice.

Statistical analysis

Data are expressed as mean ± SEM, and analyses were performed using the Prism 5.0 GraphPad Software (San Diego, CA, USA). Statistical evaluation was performed using the Student's t test or one-way ANOVA followed by Tukey's post hoc test. p value <0.05 was considered significant.

SUPPLEMENTAL INFORMATION

Supplemental Information can be found online at https://doi.org/10.1016/j.omtn.2021.01.007.

ACKNOWLEDGMENTS

The present work was supported by the National Science Foundation of China (U19A2001), Anhui Provincial Universities Natural Science Foundation (KJ2019A0233), and the University Synergy Innovation Program of Anhui Province (GXXT-2019-045). The authors thank the experts who helped us with the language problems.

AUTHOR CONTRIBUTIONS

J.L. conceived the study and designed the experiments; C.H. helped design and review the manuscript; F.T.B., Y.Z., and X.C. performed the experiments, analyzed the data, and drafted the paper; Y.Y. helped review the draft and check language problems; Y.Z. and Y.R.Y. helped collect clinical specimens; Y.F.Z., H.M.Y., and A.W. helped perform essential experiments and establish the mouse models; F.T.B., Y.Z., and X.C. performed the essential supplementary experiments and contributed to the figure design and manuscript revision. All authors approved the final version of the manuscript.

DECLARATION OF INTERESTS

The authors declare no competing interests.

REFERENCES

1. Marcellin, P., and Kutala, B.K. (2018). Liver diseases: A major, neglected global public health problem requiring urgent actions and large-scale screening. Liver Int. *38* (*Suppl 1*), 2–6.
2. Bataller, R., and Brenner, D.A. (2005). Liver fibrosis. J. Clin. Invest. *115*, 209–218.
3. Manka, P., Zeller, A., and Syn, W.K. (2019). Fibrosis in Chronic Liver Disease: An Update on Diagnostic and Treatment Modalities. Drugs *79*, 903–927.
4. Lackner, C., and Tiniakos, D. (2019). Fibrosis and alcohol-related liver disease. J. Hepatol. *70*, 294–304.
5. Kisseleva, T., Cong, M., Paik, Y., Scholten, D., Jiang, C., Benner, C., Iwaisako, K., Moore-Morris, T., Scott, B., Tsukamoto, H., et al. (2012). Myofibroblasts revert to an inactive phenotype during regression of liver fibrosis. Proc. Natl. Acad. Sci. USA *109*, 9448–9453.
6. Moran-Salvador, E., Garcia-Macia, M., Sivaharan, A., Sabater, L., Zaki, M.Y.W., Oakley, F., Knox, A., Page, A., Luli, S., Mann, J., and Mann, D.A. (2019). Fibrogenic Activity of MECP2 Is Regulated by Phosphorylation in Hepatic Stellate Cells. Gastroenterology *157*, 1398–1412.e9.
7. Tsuchida, T., and Friedman, S.L. (2017). Mechanisms of hepatic stellate cell activation. Nat. Rev. Gastroenterol. Hepatol. *14*, 397–411.
8. Dewidar, B., Meyer, C., Dooley, S., and Meindl-Beinker, A.N. (2019). TGF-β in Hepatic Stellate Cell Activation and Liver Fibrogenesis-Updated 2019. Cells *8*, 1419.
9. Peng, H., Wan, L.Y., Liang, J.J., Zhang, Y.Q., Ai, W.B., and Wu, J.F. (2018). The roles of lncRNA in hepatic fibrosis. Cell Biosci. *8*, 63.
10. Ogawa, T., Enomoto, M., Fujii, H., Sekiya, Y., Yoshizato, K., Ikeda, K., and Kawada, N. (2012). MicroRNA-221/222 upregulation indicates the activation of stellate cells and the progression of liver fibrosis. Gut *61*, 1600–1609.
11. Greene, J., Baird, A.M., Brady, L., Lim, M., Gray, S.G., McDermott, R., and Finn, S.P. (2017). Circular RNAs: Biogenesis, Function and Role in Human Diseases. Front. Mol. Biosci. *4*, 38.
12. Lasda, E., and Parker, R. (2014). Circular RNAs: diversity of form and function. RNA *20*, 1829–1842.
13. Jeck, W.R., Sorrentino, J.A., Wang, K., Slevin, M.K., Burd, C.E., Liu, J., Marzluff, W.F., and Sharpless, N.E. (2013). Circular RNAs are abundant, conserved, and associated with ALU repeats. RNA *19*, 141–157.
14. Ivanov, A., Memczak, S., Wyler, E., Torti, F., Porath, H.T., Orejuela, M.R., Piechotta, M., Levanon, E.Y., Landthaler, M., Dieterich, C., and Rajewsky, N. (2015). Analysis of intron sequences reveals hallmarks of circular RNA biogenesis in animals. Cell Rep. *10*, 170–177.
15. Wang, Z., Zhao, Y., Wang, Y., and Jin, C. (2019). Circular RNA circHIAT1 inhibits cell growth in hepatocellular carcinoma by regulating miR-3171/PTEN axis. Biomed. Pharmacother. *116*, 108932.
16. Han, D., Li, J., Wang, H., Su, X., Hou, J., Gu, Y., Qian, C., Lin, Y., Liu, X., Huang, M., et al. (2017). Circular RNA circMTO1 acts as the sponge of microRNA-9 to suppress hepatocellular carcinoma progression. Hepatology *66*, 1151–1164.
17. Yu, J., Xu, Q.G., Wang, Z.G., Yang, Y., Zhang, L., Ma, J.Z., Sun, S.H., Yang, F., and Zhou, W.P. (2018). Circular RNA cSMARCA5 inhibits growth and metastasis in hepatocellular carcinoma. J. Hepatol. *68*, 1214–1227.
18. Guo, X.Y., Chen, J.N., Sun, F., Wang, Y.Q., Pan, Q., and Fan, J.G. (2017). circRNA_0046367 Prevents Hepatoxicity of Lipid Peroxidation: An Inhibitory Role against Hepatic Steatosis. Oxid. Med. Cell. Longev. *2017*, 3960197.
19. Zhou, Y., Lv, X., Qu, H., Zhao, K., Fu, L., Zhu, L., Ye, G., and Guo, J. (2018). Preliminary screening and functional analysis of circular RNAs associated with hepatic stellate cell activation. Gene *677*, 317–323.
20. Wang, W., Dong, R., Guo, Y., He, J., Shao, C., Yi, P., Yu, F., Gu, D., and Zheng, J. (2019). CircMTO1 inhibits liver fibrosis via regulation of miR-17-5p and Smad7. J. Cell. Mol. Med. *23*, 5486–5496.
21. Chen, X., Li, H.D., Bu, F.T., Li, X.F., Chen, Y., Zhu, S., Wang, J.N., Chen, S.Y., Sun, Y.Y., Pan, X.Y., et al. (2020). Circular RNA circFBXW4 suppresses hepatic fibrosis via targeting the miR-18b-3p/FBXW7 axis. Theranostics *10*, 4851–4870.
22. Martin, J.E., Broen, J.C., Carmona, F.D., Teruel, M., Simeon, C.P., Vonk, M.C., van 't Slot, R., Rodriguez-Rodriguez, L., Vicente, E., Fonollosa, V., et al.; Spanish Scleroderma Group (2012). Identification of CSK as a systemic sclerosis genetic risk factor through Genome Wide Association Study follow-up. Hum. Mol. Genet. *21*, 2825–2835.
23. Zhuang, L.K., Yang, Y.T., Ma, X., Han, B., Wang, Z.S., Zhao, Q.Y., Wu, L.Q., and Qu, Z.Q. (2016). MicroRNA-92b promotes hepatocellular carcinoma progression by targeting Smad7 and is mediated by long non-coding RNA XIST. Cell Death Dis. *7*, e2203.
24. Lei, X.F., Fu, W., Kim-Kaneyama, J.R., Omoto, T., Miyazaki, T., Li, B., and Miyazaki, A. (2016). Hic-5 deficiency attenuates the activation of hepatic stellate cells and liver fibrosis through upregulation of Smad7 in mice. J. Hepatol. *64*, 110–117.
25. Hyun, J., Wang, S., Kim, J., Rao, K.M., Park, S.Y., Chung, I., Ha, C.S., Kim, S.W., Yun, Y.H., and Jung, Y. (2016). MicroRNA-378 limits activation of hepatic stellate cells and liver fibrosis by suppressing Gli3 expression. Nat. Commun. *7*, 10993.
26. Zhou, L., Liu, S., Han, M., Ma, Y., Feng, S., Zhao, J., Lu, H., Yuan, X., and Cheng, J. (2018). miR-185 Inhibits Fibrogenic Activation of Hepatic Stellate Cells and Prevents Liver Fibrosis. Mol. Ther. Nucleic Acids *10*, 91–102.
27. Bian, E.B., Wang, Y.Y., Yang, Y., Wu, B.M., Xu, T., Meng, X.M., Huang, C., Zhang, L., Lv, X.W., Xiong, Z.G., and Li, J. (2017). Hotair facilitates hepatic stellate cells

activation and fibrogenesis in the liver. Biochim. Biophys. Acta Mol. Basis Dis. *1863*, 674–686.

28. Zheng, Q., Bao, C., Guo, W., Li, S., Chen, J., Chen, B., Luo, Y., Lyu, D., Li, Y., Shi, G., et al. (2016). Circular RNA profiling reveals an abundant circHIPK3 that regulates cell growth by sponging multiple miRNAs. Nat. Commun. *7*, 11215.

29. He, R., Liu, P., Xie, X., Zhou, Y., Liao, Q., Xiong, W., Li, X., Li, G., Zeng, Z., and Tang, H. (2017). circGFRA1 and GFRA1 act as ceRNAs in triple negative breast cancer by regulating miR-34a. J. Exp. Clin. Cancer Res. *36*, 145.

30. Zhou, B., and Yu, J.W. (2017). A novel identified circular RNA, circRNA_010567, promotes myocardial fibrosis via suppressing miR-141 by targeting TGF-β1. Biochem. Biophys. Res. Commun. *487*, 769–775.

31. Zhou, Z., Jiang, R., Yang, X., Guo, H., Fang, S., Zhang, Y., Cheng, Y., Wang, J., Yao, H., and Chao, J. (2018). circRNA Mediates Silica-Induced Macrophage Activation Via HECTD1/ZC3H12A-Dependent Ubiquitination. Theranostics *8*, 575–592.

32. Kulcheski, F.R., Christoff, A.P., and Margis, R. (2016). Circular RNAs are miRNA sponges and can be used as a new class of biomarker. J. Biotechnol. *238*, 42–51.

33. Memczak, S., Jens, M., Elefsinioti, A., Torti, F., Krueger, J., Rybak, A., Maier, L., Mackowiak, S.D., Gregersen, L.H., Munschauer, M., et al. (2013). Circular RNAs are a large class of animal RNAs with regulatory potency. Nature *495*, 333–338.

34. Holdt, L.M., Kohlmaier, A., and Teupser, D. (2018). Molecular roles and function of circular RNAs in eukaryotic cells. Cell. Mol. Life Sci. *75*, 1071–1098.

35. Bu, F.T., Chen, Y., Yu, H.X., Chen, X., Yang, Y., Pan, X.Y., Wang, Q., Wu, Y.T., Huang, C., Meng, X.M., and Li, J. (2018). SENP2 alleviates CCl_4-induced liver fibrosis by promoting activated hepatic stellate cell apoptosis and reversion. Toxicol. Lett. *289*, 86–98.

36. Kristensen, L.S., Andersen, M.S., Stagsted, L.V.W., Ebbesen, K.K., Hansen, T.B., and Kjems, J. (2019). The biogenesis, biology and characterization of circular RNAs. Nat. Rev. Genet. *20*, 675–691.